Research Article | Vol. 7, No. 12 | 1 Dec 2017 | OPTICAL MATERIALS EXPRESS 4258
Optical Materials EXPRESS

Femtosecond-laser-written hexagonal cladding waveguide in Tm:KLu(WO$_4$)$_2$: μ-Raman study and laser operation

ESROM KIFLE,[1] PAVEL LOIKO,[2] XAVIER MATEOS,[1,3,6,*] JAVIER RODRÍGUEZ VÁZQUEZ DE ALDANA,[4] AIRAN RÓDENAS,[1,5] UWE GRIEBNER,[3] VALENTIN PETROV,[3] MAGDALENA AGUILÓ,[1] AND FRANCESC DÍAZ[1]

[1]*Física i Cristal·lografia de Materials i Nanomaterials (FiCMA-FiCNA)-EMaS, Universitat Rovira i Virgili (URV), Campus Sescelades, c/ Marcel·lí Domingo, s/n., E-43007 Tarragona, Spain*
[2]*ITMO University, 49 Kronverkskiy pr., 197101 St. Petersburg, Russia*
[3]*Max Born Institute for Nonlinear Optics and Short Pulse Spectroscopy, Max-Born-Str. 2a, D-12489 Berlin, Germany*
[4]*Aplicaciones del Láser y Fotónica, University of Salamanca, 37008 Salamanca, Spain*
[5]*Istituto di Fotonica e Nanotecnologie, Consiglio Nazionale delle Ricerche (IFN-CNR), Piazza Leonardo da Vinci, 32, 20133 Milano, Italy*
[6]*mateos@mbi-berlin.de*
[*]*xavier.mateos@urv.cat*

Abstract: We report on the fabrication, μ-Raman characterization, and continuous-wave laser operation of a channel waveguide with a hexagonal optical-lattice-like cladding fabricated in monoclinic Tm:KLu(WO$_4$)$_2$ crystal by femtosecond direct laser writing. μ-Raman spectroscopy indicates preservation of the crystalline quality in the core region and an anisotropic residual stress field. When pumped by a Ti:Sapphire laser at 802 nm, the Tm:KLu(WO$_4$)$_2$ buried channel waveguide laser generated 136 mW at 1843.7 nm with a slope efficiency of 34.2% and a threshold as low as 21 mW, which are the record characteristics for femtosecond-laser-written Tm crystalline waveguide lasers. The variation of the output coupling resulted in discrete wavelength tuning of the laser emission from 1785 to 1862 nm. The propagation losses in the waveguide are ~1.2 ± 0.3 dB/cm.

OCIS codes: (140.3380) Laser materials; (300.0300) Spectroscopy; (230.7380) Waveguides, channeled.

References and links

1. R. C. Stoneman and L. Esterowitz, "Efficient, broadly tunable, laser-pumped Tm:YAG and Tm:YSGG cw lasers," Opt. Lett. **15**(9), 486–488 (1990).
2. K. van Dalfsen, S. Aravazhi, C. Grivas, S. M. García-Blanco, and M. Pollnau, "Thulium channel waveguide laser with 1.6 W of output power and ~80% slope efficiency," Opt. Lett. **39**(15), 4380–4383 (2014).
3. K. van Dalfsen, S. Aravazhi, D. Geskus, K. Wörhoff, and M. Pollnau, "Efficient $KY_{1-x-y}Gd_xLu_y(WO_4)_2:Tm^{3+}$ channel waveguide lasers," Opt. Express **19**(6), 5277–5282 (2011).
4. S. Taccheo, G. D. Valle, R. Osellame, G. Cerullo, N. Chiodo, P. Laporta, O. Svelto, A. Killi, U. Morgner, M. Lederer, and D. Kopf, "Er:Yb-doped waveguide laser fabricated by femtosecond laser pulses," Opt. Lett. **29**(22), 2626–2628 (2004).
5. K. M. Davis, K. Miura, N. Sugimoto, and K. Hirao, "Writing waveguides in glass with a femtosecond laser," Opt. Lett. **21**(21), 1729–1731 (1996).
6. A. M. Streltsov and N. F. Borrelli, "Study of femtosecond-laser-written waveguides in glasses," J. Opt. Soc. Am. B **19**(10), 2496–2504 (2002).
7. M. Ams, G. D. Marshall, P. Dekker, J. A. Piper, and M. J. Withford, "Ultrafast laser written active devices," Laser Photonics Rev. **3**(6), 535–544 (2009).
8. J. Siebenmorgen, K. Petermann, G. Huber, K. Rademaker, S. Nolte, and A. Tünnermann, "Femtosecond laser written stress-induced Nd:$Y_3Al_5O_{12}$ (Nd:YAG) channel waveguide laser," Appl. Phys. B **97**(2), 251–255 (2009).
9. Y. Jia, C. Cheng, J. R. Vázquez de Aldana, G. R. Castillo, B. del Rosal Rabes, Y. Tan, D. Jaque, and F. Chen, "Monolithic crystalline cladding microstructures for efficient light guiding and beam manipulation in passive and active regimes," Sci Rep. **4**, 5988 (2014).
10. T. Calmano, J. Siebenmorgen, O. Hellmig, K. Petermann, and G. Huber, "Nd: YAG waveguide laser with 1.3 W output power, fabricated by direct femtosecond laser writing," Appl. Phys. B **100**(1), 131–135 (2010).

#304309 https://doi.org/10.1364/OME.7.004258
Journal © 2017 Received 22 Sep 2017; revised 24 Oct 2017; accepted 26 Oct 2017; published 7 Nov 2017

Optical Materials EXPRESS

11. Y. Tan, A. Rodenas, F. Chen, R. R. Thomson, A. K. Kar, D. Jaque, and Q. Lu, "70% slope efficiency from an ultrafast laser-written Nd:$GdVO_4$ channel waveguide laser," Opt. Express **18**(24), 24994–24999 (2010).
12. G. Salamu, F. Jipa, M. Zamfirescu, and N. Pavel, "Watt-level output power operation from diode-laser pumped circular buried depressed-cladding waveguides inscribed in Nd:YAG by direct femtosecond-laser writing," IEEE Photon. J. **8**(1), 1500209 (2016).
13. J. Siebenmorgen, T. Calmano, K. Petermann, and G. Huber, "Highly efficient Yb:YAG channel waveguide laser written with a femtosecond-laser," Opt. Express **18**(15), 16035–16041 (2010).
14. T. Calmano, J. Siebenmorgen, A.-G. Paschke, C. Fiebig, K. Paschke, G. Erbert, K. Petermann, and G. Huber, "Diode pumped high power operation of a femtosecond laser inscribed Yb:YAG waveguide laser," Opt. Mater. Express **1**(3), 428–433 (2011).
15. G. Della Valle, S. Taccheo, R. Osellame, A. Festa, G. Cerullo, and P. Laporta, "1.5 μm single longitudinal mode waveguide laser fabricated by femtosecond laser writing," Opt. Express **15**(6), 3190–3194 (2007).
16. D. G. Lancaster, S. Gross, H. Ebendorff-Heidepriem, K. Kuan, T. M. Monro, M. Ams, A. Fuerbach, and M. J. Withford, "Fifty percent internal slope efficiency femtosecond direct-written Tm^{3+}:ZBLAN waveguide laser," Opt. Lett. **36**(9), 1587–1589 (2011).
17. Y. Ren, G. Brown, A. Ródenas, S. Beecher, F. Chen, and A. K. Kar, "Mid-infrared waveguide lasers in rare-earth-doped YAG," Opt. Lett. **37**(16), 3339–3341 (2012).
18. D. G. Lancaster, S. Gross, A. Fuerbach, H. E. Heidepriem, T. M. Monro, and M. J. Withford, "Versatile large-mode-area femtosecond laser-written Tm:ZBLAN glass chip lasers," Opt. Express **20**(25), 27503–27509 (2012).
19. D. G. Lancaster, S. Gross, M. J. Withford, and T. M. Monro, "Widely tunable short-infrared thulium and holmium doped fluorozirconate waveguide chip lasers," Opt. Express **22**(21), 25286–25294 (2014).
20. E. Kifle, X. Mateos, J. R. de Aldana, A. Ródenas, P. Loiko, S. Y. Choi, F. Rotermund, U. Griebner, V. Petrov, M. Aguiló, and F. Díaz, "Femtosecond-laser-written Tm:$KLu(WO_4)_2$ waveguide lasers," Opt. Lett. **42**(6), 1169–1172 (2017).
21. X. Mateos, P. Loiko, J.M. Serres, K. Yumashev, U. Griebner, V. Petrov, M. Aguiló, and F. Díaz, "Efficient micro-lasers based on highly-doped monoclinic double tungstates," IEEE J. Quantum Electron. **53**(3), 1700110 (2017).
22. O. Silvestre, M. C. M. Rico, F. Güell, M. Aguiló, and F. Diaz, "Thulium doped monoclinic $KLu(WO_4)_2$ single crystals: growth and spectroscopy," Appl. Phys. B **87**(4), 707–716 (2007).
23. A. E. Troshin, V. E. Kisel, A. S. Yasukevich, N. V. Kuleshov, A. A. Pavlyuk, E. B. Dunina, and A. A. Kornienko, "Spectroscopy and laser properties of Tm^{3+}:$KY(WO_4)_2$ crystal," Appl. Phys. B **86**(2), 287–292 (2007).
24. O. Silvestre, J. Grau, M. C. Pujol, J. Massons, M. Aguiló, F. Díaz, M. T. Borowiec, A. Szewczyk, M. U. Gutowska, M. Massot, A. Salazar, and V. Petrov, "Thermal properties of monoclinic $KLu(WO_4)_2$ as a promising solid state laser host," Opt. Express **16**(7), 5022–5034 (2008).
25. V. Petrov, M. C. Pujol, X. Mateos, Ò. Silvestre, S. Rivier, M. Aguiló, R. M. Solé, J. H. Liu, U. Griebner, and F. Díaz, "Growth and properties of $KLu(WO_4)_2$, and novel ytterbium and thulium lasers based on this monoclinic crystalline host," Laser Photonics Rev. **1**(2), 179–212 (2007).
26. J. M. Serres, X. Mateos, P. Loiko, K. Yumashev, N. Kuleshov, V. Petrov, U. Griebner, M. Aguiló, and F. Díaz, "Diode-pumped microchip Tm:$KLu(WO_4)_2$ laser with more than 3 W of output power," Opt. Lett. **39**(14), 4247–4250 (2014).
27. M. Pollnau, Y. E. Romanyuk, F. Gardillou, C. N. Borca, U. Griebner, S. Rivier, and V. Petrov, "Double tungstate lasers: From bulk toward on-chip integrated waveguide devices," IEEE J. Sel. Top. Quantum Electron. **13**(3), 661–671 (2007).
28. F. M. Bain, A. A. Lagatsky, R. R. Thomson, N. D. Psaila, N. V. Kuleshov, A. K. Kar, W. Sibbett, and C. T. A. Brown, "Ultrafast laser inscribed Yb:$KGd(WO_4)_2$ and Yb:$KY(WO_4)_2$ channel waveguide lasers," Opt. Express **17**(25), 22417–22422 (2009).
29. X. Liu, S. Qu, Y. Tan, C. Zhang, and F. Chen, "Buried channel waveguides in neodymium-doped $KGd(WO_4)_2$ fabricated by low-repetition-rate femtosecond laser writing," Appl. Phys. B **103**(1), 145–149 (2011).
30. X. Liu, S. Qu, Y. Tan, and F. Chen, "Preservation of fluorescence and Raman gain in the buried channel waveguides in neodymium-doped $KGd(WO_4)_2$(Nd:KGW) by femtosecond laser writing," Appl. Opt. **50**(6), 930–934 (2011).
31. S. M. Eaton, C. A. Merchant, R. Iyer, A. J. Zilkie, A. S. Helmy, J. S. Aitchison, P. R. Herman, D. Kraemer, R. J. D. Miller, C. Hnatovsky, and R. S. Taylor, "Raman gain from waveguides inscribed in $KGd(WO_4)_2$ by high repetition rate femtosecond laser," Appl. Phys. Lett. **92**(8), 81105 (2008).
32. A. Ródenas, G. Zhou, D. Jaque, and M. Gu, "Direct laser writing of three-dimensional photonic structures in Nd:yttrium aluminum garnet laser ceramics," Appl. Phys. Lett. **93**(15), 151104 (2008).
33. W. Nie, Y. Jia, J. R. Vázquez de Aldana, and F. Chen, "Efficient second harmonic generation in 3D nonlinear optical-lattice-like cladding waveguide splitters by femtosecond laser inscription," Sci Rep. **6**, 22310 (2016).
34. F. Chen and J. R. Vázquez de Aldana, "Three-dimensional femtosecond laser micromachining of dielectric crystals for photonic waveguiding applications," Proc. SPIE **9532**, 95320M (2015).
35. H.-D. Nguyen, A. Ródenas, J. R. Vázquez de Aldana, J. Martínez, F. Chen, M. Aguiló, M. C. Pujol, and F. Díaz, "Heuristic modelling of laser written mid-infrared $LiNbO_3$ stressed-cladding waveguides," Opt. Express **24**(7), 7777–7791 (2016).

Optical Materials EXPRESS

36. J. A. Caird, S. A. Payne, P. R. Staber, A. J. Ramponi, L. L. Chase, and W. F. Krupke, "Quantum electronic properties of the $Na_3Ga_2Li_3F_{12}:Cr^{3+}$ laser," IEEE J. Quantum Electron. **24**(6), 1077–1099 (1988).
37. J. Morris, N. K. Stevenson, H. T. Bookey, A. K. Kar, C. T. A. Brown, J.-M. Hopkins, M. D. Dawson, and A. A. Lagatsky, "1.9 μm waveguide laser fabricated by ultrafast laser inscription in $Tm:Lu_2O_3$ ceramic," Opt. Express **25**(13), 14910–14917 (2017).
38. P. Loiko and M. Pollnau, "Stochastic model of energy-transfer processes among rare-earth ions. Example of $Al_2O_3:Tm^{3+}$," J. Phys. Chem. C **120**(46), 26480–26489 (2016).
39. J. Siebenmorgen, K. Petermann, G. Huber, K. Rademaker, S. Nolte, and A. Tünnermann, "Femtosecond laser written stress-induced $Nd:Y_3Al_5O_{12}$ (Nd:YAG) channel waveguide laser," Appl. Phys. B **97**(2), 251–255 (2009).
40. H. Liu, Q. An, F. Chen, J. R. Vazquez de Aldana, and B. del Rosal Rabes, "Continuous-wave lasing at 1.06 μm in femtosecond laser written Nd:KGW waveguides," Opt. Mater. **37**, 93–96 (2014).
41. M. C. Teich and B. E. A. Saleh, *Fundamentals of Photonics (*Canada, Wiley Interscience, 1991), Chap. 8.1.
42. F. Fusari, R. R. Thomson, G. Jose, F. M. Bain, A. A. Lagatsky, N. D. Psaila, A. K. Kar, A. Jha, W. Sibbett, and C. T. A. Brown, "Lasing action at around 1.9 μm from an ultrafast laser inscribed Tm-doped glass waveguide," Opt. Lett. **36**(9), 1566–1568 (2011).
43. Y. Y. Ren, S. J. Beecher, G. Brown, A. Ródenas, A. Lancaster, F. Chen, and A. K. Kar, "Q-switched mode-locking of a mid-infrared Tm:YAG waveguide laser with graphene film," *in Conference on Lasers and Electro-Optics Pacific Rim*, P. ThA1–3 (IEEE, 2013).

1. Introduction

Waveguide lasers emitting at ~2 μm are of interest for environmental and medical sensing applications because this spectral range contains absorption lines of many relevant organic molecules and gases. The 2 μm laser emission is usually obtained from Thulium (Tm^{3+}) or Holmium (Ho^{3+}) oscillators. In the former case, it is related to the $^3F_4 \rightarrow {}^3H_6$ electronic transition. Tm lasers can be efficiently pumped at ~0.8 μm, they exhibit high pump quantum efficiency potentially reaching 2 due to the efficient cross-relaxation (CR) process for adjacent Tm^{3+} ions and they offer broad tunability of the laser emission [1].

An efficient continuous-wave (CW) Tm waveguide laser fabricated by the Liquid Phase Epitaxy (LPE) technique has been previously demonstrated [2]. Low propagation losses (~0.11 dB/cm) in such devices were also detected at ~2 μm [3]. Femtosecond (fs) direct laser writing (DLW) is an emerging technology for production of micro-scale integrated active structures in bulk transparent dielectric materials [4–9]. This method is much less complex than the LPE or pulsed laser deposition (PLD) offering a wide range of waveguide geometries, short fabrication time, high precision and good optical quality and, hence, low propagation losses for the waveguides. Fs-DLW can be easily applied to various low-symmetry crystals exhibiting natural optical anisotropy which is challenging for LPE. Even for the crystals for which the LPE method is well-developed (i.e., including two growth steps, namely growth of a bulk crystal further serving as a substrate and growth of the epitaxial layer), fs-DLW is easier as it requires only one growth step.

To date, fs-DLW channel waveguides were realized in materials doped with several rare-earth ions, such as Nd^{3+} [8,10–12] and Yb^{3+} [13,14] at ~1 μm, Er^{3+} at ~1.5 μm [15] and Tm^{3+} at ~2 μm [16,17]. At ~1 μm, very high CW laser slope efficiencies η were reached. In [13], a fs-DLW Yb:YAG waveguide laser generated 765 mW at 1.03 μm with a record η = 75% and in [11], a $Nd:GdVO_4$ laser generated 256 mW at 1.06 μm with η = 70%. Watt-level output from a diode-pumped fs-DLW Nd:YAG ceramic laser was demonstrated at ~1.06 μm and at 1.3 μm [12]. There are only sporadic reports on Tm fs-DLW waveguide lasers in the literature which were devoted to Tm^{3+}-doped ZBLAN glasses and YAG crystals (i.e., isotropic materials) [16–20]. In [18], a fs-DLW Tm:ZBLAN laser generated 205 mW at 1.89 μm with η = 67%.

The monoclinic double tungstate (MDT) laser host crystals with general formula $KRE(WO_4)_2$ or shortly KREW where RE = Gd, Y or Lu are known for providing high doping concentrations [21], high transition cross-sections [22,23], and minimal fluorescence quenching for different rare-earth dopants at acceptable thermal properties [24,25] which makes them very suitable for efficient bulk [25], thermo- [26] and index-guided [27] lasers. However, only one report could be found in the literature on Yb^{3+}-doped KGdW and KYW

Optical Materials EXPRESS

fs-DLW waveguide lasers [28] where the Yb:KGdW laser generated 18.6 mW at 1023 nm with η = 9.3%. Nd^{3+}-doped KGdW fs-DLW waveguides were characterized in [29,30] but no lasing was demonstrated. Raman gain from the fs-DLW waveguide in undoped KGdW was observed in [31].

Very recently, we reported on the development and CW laser performance of fs-DLW Tm:KLuW channel waveguides with a circular cladding [20]. In the present paper, we demonstrate a fs-DLW Tm:KLuW channel waveguide with a hexagonal optical-lattice-like [32–34] cladding. We present results of μ-Raman and emission spectroscopy, and CW laser operation at 1.78-1.86 μm. This type of fs-DLW waveguides which can be described as type II modification with type III cladding geometry [34] are advantageous because they can be potentially used for the creation of fully 3D fs-DLW micro-structures in anisotropic crystals allowing for light propagation in any direction (along the waveguide), and tailoring the spatial profile of the light beam, e.g. in beam splitters, for simultaneous generation and manipulation of the laser beam [9,33,34].

2. Waveguide fabrication

Depressed-index waveguides were fabricated in a bulk Tm:KLuW crystal by 3D fs-DLW. The crystal itself was grown by the Top-Seeded-Solution Growth (TSSG) Slow-Cooling method [25]. It was doped with 3 at.% Tm^{3+} (N_{Tm} = 2.15 × 10^{20} at/cm^3). A rectangular 3.0 mm-thick sample was cut from this crystal oriented for light propagation along the N_g optical indicatrix axis (KLuW is an optically biaxial crystal). Its aperture was 3.10 (N_m) × 2.85 (N_p) mm^2 and both N_m × N_p faces were polished to laser-grade quality.

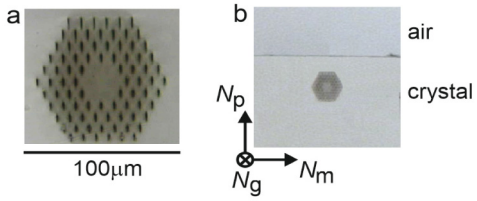

Fig. 1. (a,b) Bright-field microscope images of the facet cross-section of the fs-DLW hexagonal cladding Tm:KLuW waveguide.

For DLW, 120-fs, 795 nm pulses from a Ti:Sapphire regenerative amplifier (Spitfire, Spectra Physics) were used employing a small fraction of the output energy at 1 kHz repetition rate. The laser beam was focused into the crystal with a 40 × microscope objective (N.A. = 0.65). The incident pulse energy on the crystal was set to 73 nJ, with the help of a half-wave plate, a polarizer and a calibrated neutral density (ND) filter. It was kept constant during the inscription. The crystal was scanned at a constant speed of 300 μm/s along the N_g-axis thus producing damage tracks. The polarization of the fs laser ($E \parallel N_m$) was perpendicular to the scanning direction to avoid anisotropic effects related to the birefringence of DTs. The line scan procedure was repeated at different depths and lateral positions of the sample. The channel waveguide consisted of a 30 μm diameter core and four hexagonal-shaped groups of damage tracks forming a hexagonal cladding, see Fig. 1(a). The axis of the waveguide was located 120 μm beneath the crystal surface, Fig. 1(b). The separation between adjacent tracks was 8 μm and 3 μm (in horizontal and vertical directions, respectively).

3. Waveguide characterization

3.1 Luminescence

At first, we studied the luminescence from the waveguide core. For this, the output of a CW Ti:Sapphire laser (Coherent, model MIRA 900) tuned to ~802 nm ($^3H_6 \rightarrow {}^3H_4$ transition of Tm^{3+}) was coupled into the waveguide using a 10 × microscope objective lens (Mitutoyo M

Optical Materials EXPRESS

Plan Apo, numerical aperture, N.A.: 0.28, focal length: 20 mm). The Tm^{3+} luminescence was collected from the output facet of the waveguide using a Glan-Taylor polarizer and an optical fiber, and detected with an optical spectrum analyzer (OSA, Yokogawa, model AQ6375B), Fig. 2(a). The fabricated waveguide exhibited intense luminescence related to the $^3F_4 \rightarrow {}^3H_6$ transition of Tm^{3+} with a notable anisotropy for the light polarizations $E \parallel N_m$ and $E \parallel N_p$ which is a prerequisite for linearly polarized laser output.

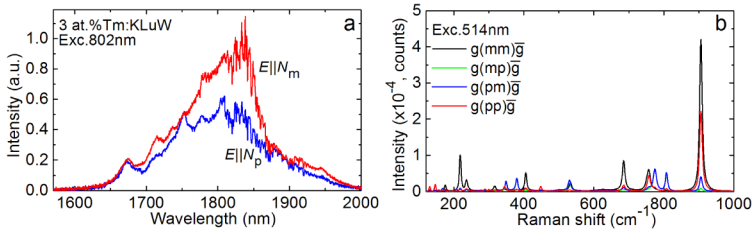

Fig. 2. (a) $^3F_4 \rightarrow {}^3H_6$ luminescence of Tm^{3+} ions from the fs-DLW Tm:KLuW waveguide for light polarizations $E \parallel N_m$ and N_p, λ_{exc} = 802 nm; the noise at 1.8-1.9 μm is due to the water absorption in air, and (b) polarized Raman spectra of the waveguide core region measured in backscattering geometry, λ_{exc} = 514 nm.

3.2 μ-Raman study

To characterize the modification of the crystal structure in the waveguide core and cladding, a μ-Raman analysis was performed. A Renishaw inVia Reflex confocal Raman microscope equipped with a 514 nm Ar^+ laser and a 50 × Leica objective was used. The facet cross-section of the waveguide was studied with a spatial resolution of 0.4 μm. The polarization of the excitation laser was $E \parallel N_m$. We analyzed two intense high-frequency phonon modes, namely the 907.6 cm^{-1} internal mode, assigned as ν(W–O)/ν_1 and related to the W–O stretching vibrations in the distorted WO_6 octahedrons [25], and the 686.5 cm^{-1} mode, assigned as ν(WOOW) * ν(W–O)/ν_3 and related to the double oxygen bridge stretching vibrations [25]. While the 907.6 cm^{-1} mode is typical for all simple and complex tungstate crystals and it is the most intense one for KLuW, the second mode is characteristic for MDTs and it is not observed for isolated WO_4 tetrahedrons, e.g. in tetragonal scheelite-type tungstates. The polarized Raman spectra measured in the core region are shown in Fig. 2(b).

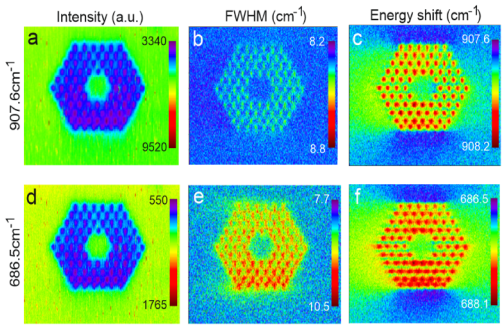

Fig. 3. Micro-Raman mapping of the facet cross-section of the fs-DLW hexagonal cladding Tm:KLuW waveguide at 907.6 cm^{-1}: (a) peak intensity, (b) full width at half maximum (FWHM) and (c) phonon energy shift. Similar maps are given for the Raman band at 686.5 cm^{-1} in (d) peak intensity, (e) FWHM and (f) phonon energy shift.

The μ-Raman analysis results are summarized in Fig. 3. We analyzed the peak intensity, Fig. 3(a,d), full width at half maximum (FWHM), Fig. 3(b,e), and the peak position for the 907.6 cm^{-1} and 686.5 cm^{-1} Raman bands, Fig. 3(c,f). In the core region, the crystalline quality of the material is preserved because the intensity of the Raman bands in the core and in the

Optical Materials EXPRESS

bulk crystal volume is the same, see Fig. 3(a,d). This feature confirms the feasibility of the produced waveguide for laser operation. The cladding region consists of a slightly damaged material indicated by the decreased intensity, broadening and shift of the phonon mode. The two latter effects are especially pronounced for the 686.5 cm^{-1} mode which is characteristic of the MDT structure. The existence of a residual anisotropic stress field is evident from the observed phonon energy shift outside the cladding, see Fig. 3(c,f). This stress field leads to birefringence due to the photo-elastic effect and favors the polarization-selective response of the waveguide [35].

In Fig. 4, we analyzed the variation of the peak intensity and the peak position of the two studied Raman modes along a horizontal line going through the center of the waveguide cross-section. It supports our previous conclusion about the weak alteration of the material structure in the core and allows one to clearly see the effect of four tracks forming the cladding from both sides of the core.

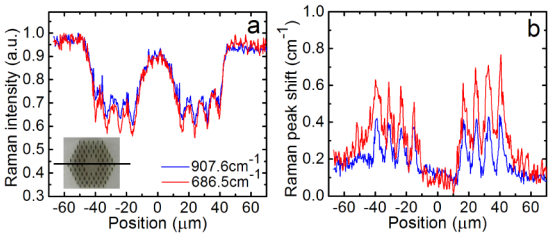

Fig. 4. Variation of the Raman intensity (a) and Raman peak shift (b) along the cross-section of the fs-DLW hexagonal cladding Tm:KLuW waveguide, as shown in the *inset* of (a), for the 907.6 cm^{-1} and 686.5 cm^{-1} Raman bands. The Raman peak shift in (b) is calculated with respect to the bulk (non-damaged) material.

4. Continuous-wave laser operation

4.1 Laser set-up

The Tm:KLuW sample containing the fs-DLW waveguide was placed on a passively-cooled flint glass substrate. The laser cavity consisted of a flat pump mirror (PM) that was antireflection (AR) coated for 0.7–1.0 μm and high-reflection (HR) coated for 1.8–2.1 μm and a flat output coupler (OC) having a transmission of T_{OC} = 1.5%, 3%, 5%, 9%, 20% or 30% at 1.8–2.1 μm. Additionally, we tested a high-transmission (T_{OC} = 80% at 1.78 μm) "bandpass" OC coated to support laser operation at <1.8 μm. Both PM and OC were placed close to the sample faces with minimum air gaps. No index-matching liquid was used to avoid laser-induced damage of the waveguide or mirror faces as observed in our first experiments. Laser operation without an OC relying on Fresnel reflection on an uncoated surface (T_{OC} = 89% at 1.84 μm, the corresponding refractive index n_m is 1.995) was also studied. As a pump source, we used the CW Ti:Sapphire laser (Section 3.1). The polarization of the pump beam corresponded to $E \parallel N_m$ in the crystal. The pump was coupled into the waveguide with a 10 × microscope objective lens (Section 3.1). The incident pump power was varied with a gradient ND filter placed before the objective. The pump beam radius w_p in the focus was ~20 μm. The pump absorption under lasing conditions (single pass pumping), denoted as *Abs*, was ~75% (for T_{OC} < 30%) and ~48% (for T_{OC} = 80% and 89%), see the details below. The scheme of the laser set-up is shown in Fig. 5(a). The Tm:KLuW waveguide under lasing conditions exhibited a weak blue upconversion luminescence, Fig. 5(b).

Optical Materials EXPRESS

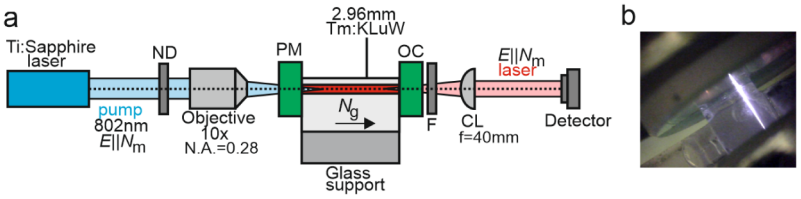

Fig. 5. (a) Scheme of the fs-DLW Tm:KLuW channel waveguide laser: PM – pump mirror, OC – output coupler, ND – neutral density filter, F – long-pass filter, CL – collimating lens; (b) top view of the pumped Tm:KLuW waveguide showing blue upconversion luminescence.

The laser output was filtered from the residual pump with a long-pass filter (Thorlabs, FEL1000, transmission at the laser wavelength: ~83%, transmission at the pump wavelength: < 0.01%) and collimated with an aspherical uncoated plano-convex 40 mm lens. The laser output power was measured with a sensitive Ophir Nova P/N 1Z01500 powermeter, the emission spectrum was measured using the above mentioned OSA (Section 3.1) and the beam profile was captured using a FIND-R-SCOPE near-IR camera (model 85726, sensitivity: 0.4-2.2 μm). To determine the equivalent size of the laser mode at the output facet of the waveguide, it was replaced by a 1951 USAF resolution test target (Thorlabs, model R1DS1).

4.2 Laser performance

Laser operation with the developed waveguide was achieved for all OCs and without the OC. The laser output was linearly polarized, $E \parallel N_m$, the polarization was naturally-selected by the anisotropy of the gain. The input-output dependences are shown in Fig. 6. The maximum output power was 136 mW at 1843.7 nm with a slope efficiency η of 34.2% (with respect to the absorbed pump power, P_{abs}) for T_{OC} = 30%, Fig. 6(a). The laser threshold was as low as 21 mW and the optical-to-optical efficiency η_{opt} was ~12% (with respect to the incident pump power). For smaller T_{OC}, the laser performance was inferior. Without the OC (T_{OC} = 89%), the laser generated 46 mW at 1842.6 nm with a decreased η of 20.9% and increased laser threshold of ~35 mW, Fig. 6(b). The deterioration of the laser performance for high output coupling is probably related to stronger upconversion due to the increased population of the upper laser level. The output dependences are clearly linear indicating no detrimental thermal effects; no thermally-induced cracks or damage of the crystal faces were observed.

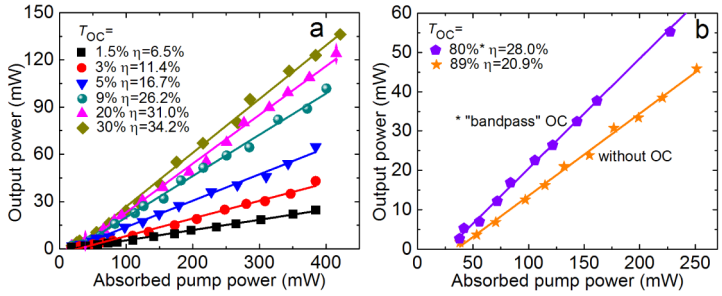

Fig. 6. Input-output dependences of the fs-DLW hexagonal cladding Tm:KLuW channel waveguide laser: (a) T_{OC} = 1.5%...30% at 1.8–2.1 μm, (b) T_{OC} = 80% (“bandpass” OC) or 89% (without an OC), η – slope efficiency.

The typical laser emission spectra measured at maximum P_{abs} (the spectra were weakly dependent on the pump level) are shown in Fig. 7. For T_{OC} <10%, multi-peak spectral behavior has been observed due to the relatively broad gain spectra of Tm^{3+} in KLuW [25]. With the increase of T_{OC} from 1.5% to 30%, the emission wavelength shifted from ~1862 to 1843.7 nm. Without the OC (for T_{OC} = 89%), the laser operated at even shorter wavelength, 1842.6 nm. Such a spectral behavior is related to the quasi-three-level nature of the Tm^{3+} laser

Optical Materials EXPRESS

and it agrees with the gain spectra of Tm^{3+} [25]. For the "bandpass" OC (for T_{OC} = 80%), the laser emission was at 1784.5 nm. It should be noted that for Tm^{3+}-doped MDT waveguides, even longer emission wavelengths (up to ~1.94 μm [3]) are possible.

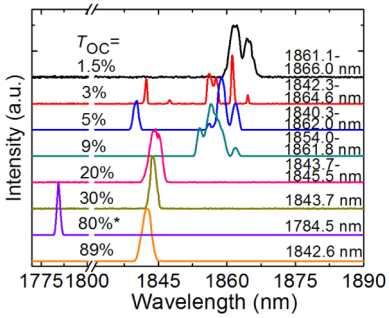

Fig. 7. Typical emission spectra for the fs-DLW hexagonal cladding Tm:KLuW channel waveguide laser (measured at the maximum P_{abs}).

To determine the propagation losses in the developed waveguide, we employed the Caird analysis [36] modified for the case of high T_{OC} [37]. The dependence of the slope efficiency on T_{OC} and the internal loss L per pass is expressed as $1/\eta = 1/\eta_0(1 + 2\gamma/\gamma_{OC})$, where $\gamma = -\ln(1 - L)$ and $\gamma_{OC} = -\ln(1 - T_{OC})$, and η_0 is an intrinsic slope efficiency. Figure 8(a) shows a plot of the inverse of the slope efficiency *versus* the inverse of γ_{OC} (excluding the data for T_{OC} = 80% and 89% for which the laser performance is affected by strong upconversion). This fit yields $\eta_0 = 65 \pm 4\%$ and $2\gamma = 0.17 \pm 0.03$ or an equivalent propagation loss coefficient, $\delta = 4.34L/l = 1.2 \pm 0.3$ dB/cm. This value is slightly lower than that for the fs-DLW Tm:KLuW waveguides with a circular cladding (~1.4 dB/cm) [20] and the fs-DLW Yb:KGdW based on a pair of damage tracks (~1.9 dB/cm) [28].

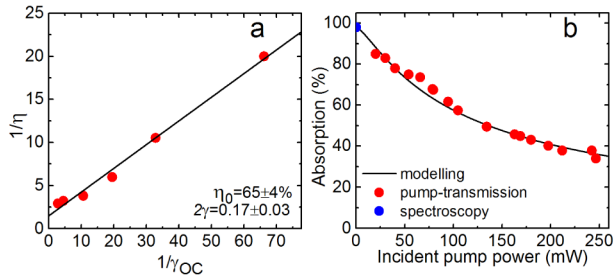

Fig. 8. fs-DLW hexagonal cladding Tm:KLuW channel waveguide laser: (a) modified Caird analysis for T_{OC} = 1.5%...30% (*circles* – experimental data, *line* – their linear fit) (b) absorption saturation in the waveguide under non-lasing conditions: *red circles* – experimental data from the pump-transmission measurement, *blue circle* – small-signal absorption from the spectroscopic data, *solid curve* – rate-equation modelling.

By employing the pump-transmission measurements under non-lasing conditions at 802 nm and at 830 nm (out of the Tm^{3+} absorption), we determined the pump coupling efficiency, $\eta_{coupl} = 49 \pm 5\%$ and pump absorption, *Abs*. Here, the value of η_{coupl} includes the Fresnel loss (~89%) on the uncoated input facet. The moderate pump coupling efficiency arises mostly from the factor of geometrical overlap of the waveguide core (diameter: 30 μm) and the pump spot size ($2w_p$ = 40 μm). *Abs* is the ratio of the absorbed pump power to the launched one. It is plotted in Fig. 8(b). Here, the blue circle is the small-signal value calculated from the spectroscopic parameters, $Abs = 1 - \exp(-\sigma_{abs}N_{Tm}l) = 98\%$, where $\sigma_{abs} = 6.2 \times 10^{-20}$ cm^2 is the absorption cross-section of Tm^{3+} ions for $E \parallel N_m$, and the red circles are the result of the pump-transmission experiment which represent the depopulation of the $^3H_6$ ground-state and,

Optical Materials EXPRESS

hence, saturation of the ground-state absorption. These data were modelled using a simple rate-equation model including the ground-state ($^3H_6$), the pump level ($^3H_4$, unquenched lifetime τ_{30} = 240 μs [21]) and the upper laser level ($^3F_4$, fluorescence lifetime τ_1 = 1.34 ms [25]). The CR for the adjacent Tm^{3+} ions, $^3H_4(Tm_1) + {}^3H_6(Tm_2) \rightarrow {}^3F_4(Tm_1) + {}^3F_4(Tm_2)$ was also accounted for using a macroscopic CR rate-constant $W_{CR} = C_{CR}N_{Tm}$ [38], where C_{CR} = 2.7 × 10^{-37} cm^6/s [21]. The results are shown in Fig. 8(b) by a black curve and they are in good agreement with the experimental data. The data from Fig. 8(b) were used to determine the pump power absorbed in the waveguide under lasing conditions for each OC.

The results on the spatial profile of the output laser beam from the waveguide laser are shown in Fig. 9. The 2D profile of the beam is nearly circular, Fig. 9(a). The comparison of the size of the laser mode at the output facet of the waveguide with the waveguide cross-section, Fig. 9(b), shows the confinement of the laser mode and its penetration into the first layer of the cladding while the mode almost completely decays at the outer hexagonal-shaped sequence of damage tracks. The 1D mode profiles were very well fitted with a Gaussian distribution, Fig. 9(c). The goodness of the Gaussian fit R^2 is 0.98. A slight ellipticity of the laser beam ($e = w_L(p)/w_L(m)$ = 1.06) which is expanded along the vertical direction (|| N_p-axis) was detected. This is attributed to the residual anisotropic stress field formed during the fs-DLW, Fig. 3(c,f).

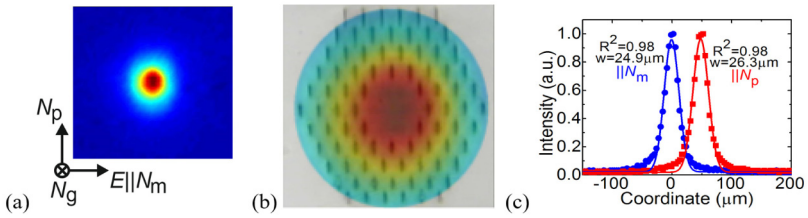

Fig. 9. Spatial profile of the output laser mode from the fs-DLW hexagonal cladding Tm:KLuW channel waveguide laser (T_{OC} = 30%, P_{abs} = 188 mW): (a) 2D profile measured in the far-field, E is the laser polarization; (b) spatial overlap of the waveguide cross-section and the reconstructed beam profile at the output facet of the waveguide; (c) the corresponding 1D profiles of the laser mode in the horizontal (|| N_m) and vertical (|| N_p) directions.

The divergence of the output laser beam θ (half-angle) was similar along the directions of N_m and N_p axes and amounted to 0.050 ± 0.005 (as measured for T_{OC} = 30% at the maximum pump power). Using the approximation of a step-index waveguide, $N.A.^2 \approx 2n_{core}\Delta n$, where N.A. = sin$\theta$ is the numerical aperture of the waveguide and $n_{core} = n_m$ is its refractive index in the core region [39,40], we estimated the variation of the refractive index in the cladding region Δn as ~6 × 10^{-4}. This allowed us to conclude about the transverse mode structure. Using the step-index approximation, we calculated the normalized frequency $V = 2\pi a \cdot N.A./\lambda_L$ [41] as 2.56 for λ_L = 1.84 μm and a waveguide core radius a of 15 μm. The cut-off V parameters for the $LP_{lm} = LP_{01}$, LP_{11} and LP_{02} modes are 0, 2.405 and 3.832, respectively, so that for a linear laser polarization, three modes are expected (LP_{01} and LP_{11}, note that the latter has a degeneracy of 2 because of its azimuthal index $l > 0$). This explains the determined values of the mode radii w_L, Fig. 9(c), which are larger than those expected for the LP_{01} mode.

The slope efficiency of the developed laser can be represented as $\eta_{calc} = \eta_{mode}\eta_{St}\eta_q\eta_{out}$ [2] (further analysis applies to T_{OC} = 9% for which the detrimental effect of upconversion is expected to be weak), where $\eta_{mode} < 1$ is the mode-matching efficiency, $\eta_{St} = \lambda_p/\lambda_L$ = 0.43 is the Stokes efficiency, η_q = 1.75 for the given N_{Tm} is the pump quantum efficiency accounting for CR, and $\eta_{out} = \ln[1-T_{OC}]/\ln[(1-T_{OC})\cdot(1-2L)]$ = 0.34 is the cavity out-coupling efficiency. Thus, the theoretical η_{calc} = 26% which is in agreement with the observed value, Fig. 6(a), indicating very high mode-matching efficiency. For higher T_{OC}, stronger discrepancy between

Optical Materials EXPRESS

the calculated and measured slope efficiency is observed due to the upconversion losses being enhanced with the inversion ratio and, consequently, with T_{OC}.

Table 1. Output Characteristics* of Femtosecond-Laser-Written Thulium Waveguide Lasers Reported So Far

Material	Pumping	λ_p, nm	P_{th}, mW	P_{out}, mW	λ_L, nm	η, %	η_{coupl}, %	Ref.
				Glasses				
Tm:ZBLAN	diode	790	21	47	1880	50^{Inc}	77	[16]
Tm:ZBLAN	Ti:Sa	790	75	132	~1900	50^{Abs}	**82**	[19]
Tm:ZBLAN	diode	791	265	60	~1900	54^{Abs}	77	[19]
Tm:ZBLAN	Ti:Sa	790	**12**	**205**	1890	$\mathbf{67}^{Abs}$	79	[18]
Tm:GPNG	Ti:Sa	791	80	32	1930	6^{Inc}	4	[42]
				Crystals/Ceramics				
$Tm:YAG^{Ceram}$	Ti:Sa	800	312	93.2	1985	27^{Inc}	20	[17]
$Tm:YAG^{Cryst}$	Ti:Sa	-	100	48	1985	12^{Inc}	9	[43]
$Tm:Lu_2O_3^{Ceram}$	Ti:Sa	796	50	81	1942	7^{Inc}	40	[37]
$Tm:KLuW^{Cryst}$	Ti:Sa	802	21	46	1912	15^{Abs}	-	[20]
$Tm:KLuW^{Cryst}$	Ti:Sa	802	**21**	**136**	1844	$\mathbf{34}^{Abs}$	**49**	This paper

*Material: *Ceram* and *Cryst* superscripts stand for the ceramics and single crystal, respectively, λ_p – pump wavelength, P_{th} – laser threshold, P_{out} – output power, λ_L – laser wavelength, η – slope efficiency (superscript: calculated versus the incident (*Inc*) or absorbed (*Abs*) pump power), η_{coupl} – pump coupling efficiency.

In Table 1, we summarized the results achieved recently with the fs-DLW Tm waveguide lasers. The output characteristics (output power, laser threshold, and slope efficiency) achieved in the present work for hexagonal cladding fs-DLW Tm:KLuW waveguide are superior with respect to the previously reported data for the fs-DLW Tm waveguide lasers based on crystalline/ceramic materials.

5. Conclusion

MDTs doped with Tm^{3+} ions are suitable for the development of fs-laser-written waveguide lasers. In the present work, we successfully fabricated, characterized and demonstrated CW laser operation of a fs-laser-written Tm:KLuW buried channel waveguide laser with a specific hexagonal optical-lattice-like cladding. This laser delivered a maximum output power of 136 mW at 1843.7 nm with a slope efficiency of 34.2% with respect to the absorbed pump power corresponding to a nearly-Gaussian laser mode. The developed waveguide is characterized by a low laser threshold 21 mW and moderate propagation losses, ~1.2 ± 0.3 dB/cm. Moreover, by applying variable output coupling, a discrete wavelength tuning from ~1785 to 1862 nm was observed. Further improvement of the slope efficiency and power scaling of fs-laser-written Tm^{3+}-doped MDT waveguide lasers is possible with the optimization of the waveguide geometry (e.g., number of track layers between 1 and 4) and fabrication conditions (e.g., pulse energy, scanning speed and track separation, which can be critical as Tm^{3+} ions absorb at the emission wavelength of the fs laser), and the use of butt-coupled mirrors. Since efficient laser operation is possible with highly-doped (up to 15 at.%) Tm^{3+}-doped MDTs [21], the fabrication of very compact integrated lasers is feasible.

Funding

Spanish Government (MAT2016-75716-C2-1-R (AEI/FEDER,UE); MAT2013-47395-C4-4-R, TEC 2014-55948-R, FIS2013-44174-P, FIS2015-71933-REDT); Junta de Castilla y León (UIC016, SA046U16); Generalitat de Catalunya (2014SGR1358).

Acknowledgments

E. K. acknowledges financial support from the Generalitat de Catalunya under grants 2016FI_B00844 and 2017FI_B100158. F.D. acknowledges additional support through the

Optical Materials EXPRESS

ICREA academia award 2010ICREA-02 for excellence in research. X. M. acknowledges support from the European Union's Horizon 2020 research and innovation programme under the Marie Skłodowska-Curie grant agreement No 657630. A. R. acknowledges funding from the European Union's Horizon 2020 research and innovation programme under the Marie Skłodowska-Curie Individual Fellowship Grant Agreement No. 747055. P. L. acknowledges financial support from the Government of the Russian Federation (Grant 074-U01) through ITMO Post-Doctoral Fellowship scheme.